



Gold-implanted plasmonic quartz plate as a launch pad for laser-driven photoacoustic microfluidic pumps

Shuai Yue^{a,b,1}, Feng Lin^{a,b,1}, Qihui Zhang^{b,c,1}, Njumbe Epie^d, Suchuan Dong^e, Xiaonan Shan^b, Dong Liu^f, Wei-Kan Chu^d, Zhiming Wang^{a,2}, and Jiming Bao^{b,2}

^aInstitute of Fundamental and Frontier Sciences, University of Electronic Science and Technology of China, Chengdu, 610054 Sichuan, China; ^bDepartment of Electrical and Computer Engineering, University of Houston, Houston, TX 77204; ^cDepartment of Electrical Information Engineering, Henan University of Engineering, Xinzheng, 451191 Henan, China; ^dPhysics Department and Texas Center for Superconductivity, University of Houston, Houston, TX 77204; ^eDepartment of Mathematics, Purdue University, West Lafayette, IN 47907; and ^fDepartment of Mechanical Engineering, University of Houston, Houston, TX 77204

Edited by Naomi J. Halas, Rice University, Houston, TX, and approved February 14, 2019 (received for review November 5, 2018)

Enabled initially by the development of microelectromechanical systems, current microfluidic pumps still require advanced micro-fabrication techniques to create a variety of fluid-driving mechanisms. Here we report a generation of micropumps that involve no moving parts and microstructures. This micropump is based on a principle of photoacoustic laser streaming and is simply made of an Au-implanted plasmonic quartz plate. Under a pulsed laser excitation, any point on the plate can generate a directional long-lasting ultrasound wave which drives the fluid via acoustic streaming. Manipulating and programming laser beams can easily create a single pump, a moving pump, and multiple pumps. The underlying pumping mechanism of photoacoustic streaming is verified by high-speed imaging of the fluid motion after a single laser pulse. As many light-absorbing materials have been identified for efficient photoacoustic generation, photoacoustic micropumps can have diversity in their implementation. These laser-driven fabrication-free micropumps open up a generation of pumping technology and opportunities for easy integration and versatile microfluidic applications.

microfluidic pumps | photoacoustics | laser streaming | ion implantation | surface plasmon resonance

A micropump is the heart of any microfluidic device and has wide applications in basic research and technological advancement (1–4). Based on their operating principle, micropumps can be divided into two groups: mechanical and nonmechanical (1, 4). Developed in the 1980s with the emergence of microelectromechanical systems, a mechanical micropump is a miniaturized version of a macroscopic pump, made of moving parts such as valves and membranes that can displace fluid directly. Although nonmechanical micropumps have no moving parts, they still require carefully fabricated microstructures and electrical contacts to generate thermal, electrical, magnetic, or acoustic stimulus to drive the fluids (1–4). While the performance of micropumps improved as the fabrication technique evolved, the principle and design of micropumps have remained almost the same over past decades (1–4). Here we report a micropump and an operating principle and design. It has no moving parts or electrodes, thus requires no micro- or nanofabrication. Furthermore, unlike previous micropumps, the size, number, location, and timing of our micropumps can be remotely controlled, reconfigured, and programmed in real time, which make them more accessible for a wide range of fluid applications.

This pump is a semitransparent plasmonic quartz window; it is based on our recently discovered principle of photoacoustic laser streaming: an ultrasound wave generated by a resonant laser pulse drives fluid through acoustic streaming (5–9). Because the whole surface of the quartz window is covered with a plasmonic layer, an ultrasound wave can be generated from any point on the window, making it a micropump launch pad. This photoacoustic window overcomes major shortcomings of previous photoacoustic cavities which had to be created individually by the same laser beam (5); it has allowed us to verify the

underlying pumping mechanism and to explore the interaction of fluids with laser and ultrasound in an unprecedented time-space regime (5–11).

Results and Discussion

The photoacoustic launch pad was created by Au ion implantation in a 0.5-mm-thick quartz window at 60 keV to a dose of 6×10^{16} per cm square (12–16). The acceleration voltage was chosen so that Au ions are implanted within 50 nm below the surface (12). A relatively high dose was used so that a sufficient Au nanoparticle concentration and corresponding optical absorption can be obtained. Fig. 1A (*Inset*) shows an optical picture of the quartz with the reddish implanted region in the center, the characteristic color of gold nanoparticles. The absorption spectrum in Fig. 1A indicates a clear peak absorption near 530 nm due to surface plasmon resonance of Au clusters and nanoparticles (16–18). To use the window as a micropump launch pad, we filled the cuvette with the deionized water without Au nanoparticles (5), and placed the quartz in a 1-cm square glass cuvette with a tunable tilt angle (Fig. 1B and C). A 527-nm pulsed laser (150-ns pulse width) was focused (10-cm focal length lens) on the quartz window instead of the cuvette wall to generate photoacoustic waves and jets (5). Red fluorescent polymer microspheres (catalog no. R0300, 3.2 μ m, emission wavelength: 612 nm; Thermo Scientific) and a 633-nm HeNe laser were used to image the motion of water with a high-speed color camera (PixelINK PL-B742U). Photoacoustic waves were

Significance

A revolutionary microfluidic pump is demonstrated; it has no moving parts and no electrical contacts. It consists of a quartz plate implanted by Au particles where every point on the plate can function as a micropump. The pump is driven by a laser beam and is based on the discovered principle of photoacoustic laser streaming. When a pulsed laser hits the plate, it is absorbed by Au nanoparticles that generate an ultrasound wave, which then drives the fluid via acoustic streaming. Because laser beams can be arbitrarily patterned and timed, the fluid can be controlled by laser in a fashion similar to musical water fountains. Such a laser-driven photoacoustic micropump will find wide applications in microfluidics and optofluidics.

Author contributions: S.Y., F.L., Q.Z., S.D., X.S., D.L., W.-K.C., Z.W., and J.B. designed research; S.Y., F.L., Q.Z., and N.E. performed research; S.Y., F.L., Q.Z., N.E., and J.B. analyzed data; and J.B. wrote the paper.

The authors declare no conflict of interest.

This article is a PNAS Direct Submission.

This open access article is distributed under [Creative Commons Attribution-NonCommercial-NoDerivatives License 4.0 \(CC BY-NC-ND\)](https://creativecommons.org/licenses/by-nc-nd/4.0/).

¹S.Y., F.L., and Q.Z. contributed equally to this work.

²To whom correspondence may be addressed. Email: zhmwang@uuestc.edu.cn or jbao@uh.edu.

Published online March 14, 2019.

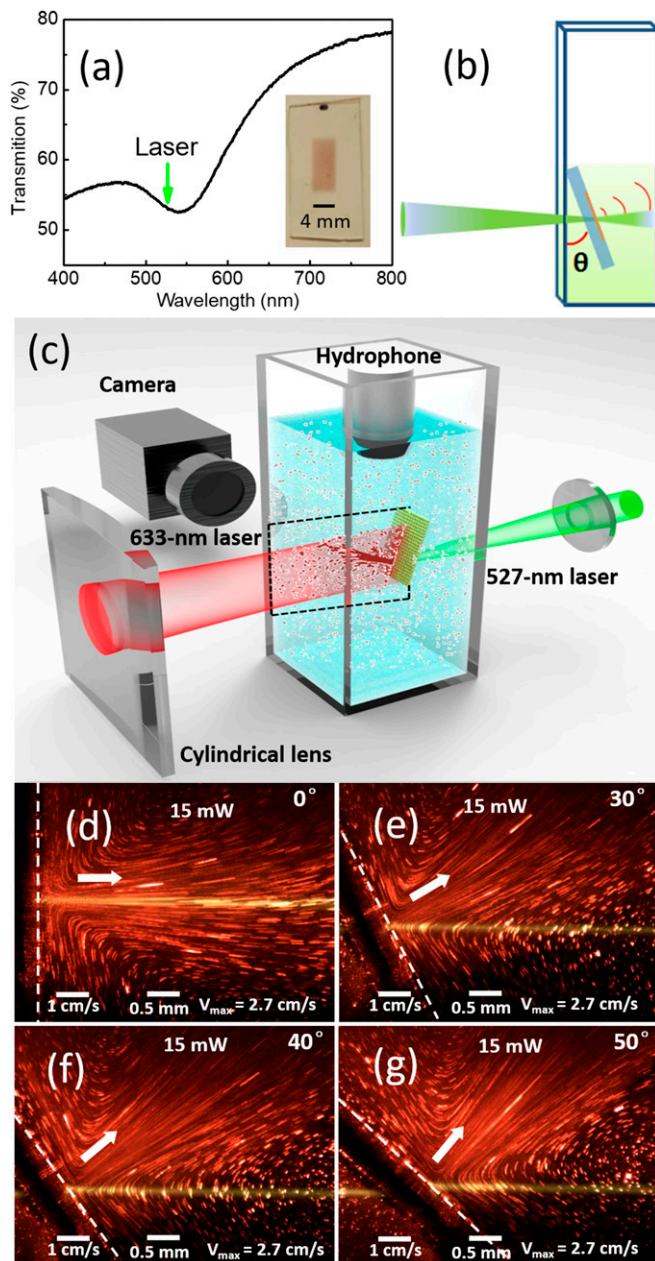


Fig. 1. Au-ion-implanted quartz window and jets launched from the window. (A) UV-visible absorption spectrum of the implanted window. (Inset) Optical picture of the quartz window. Reddish area in the center is the implanted region. (B and C) Schematics of the experimental setup to generate jets at different angles between an excitation laser beam and the quartz window. (D–G) Snapshots of jets at the incident angles of 0°, 30°, 40°, and 50°. Dashed white lines indicate the window surface in contact with water; the horizontal yellow rays are laser beams due to fluorescence from microspheres under 527-nm green light excitation.

detected by a hydrophone (V312-SU-F0.46-IN-PTF from Olympus, 10-MHz bandwidth), and then amplified by a preamplifier before being recorded by a high-speed oscilloscope (Tektronix TDS3052) (5). Unless otherwise stated, a long-pass filter was used to block 527-nm light for flow imaging; the laser repetition rate is 1,000 Hz (5).

Surprisingly, micropumps are ready to work when the jets are created by incident laser pulses from an arbitrary point on the window. Fig. 1 D–G shows snapshots of jets of the quartz

substrate for four different tilt angles. Unlike previous jets created by self-formed photoacoustic cavities (5), the jets launched by this micropump from the quartz window always flow normal to the window surface regardless of the direction of laser beams. A simple conclusion from this observation is that the jets are not driven by momentum transfer from incident photons (19, 20). Because the laser-induced heating and subsequent photothermal expansion of Au-implanted quartz layer do not depend on the angle of incident lasers, the observation of jets perpendicular to the surface agrees with the mechanism of photoacoustic streaming and does not contradict previous observations (5). On the other hand, this window–jet relationship makes it easy for the micropump to pump fluids in the same direction without worrying about the direction of a laser beam; the direction of pumping can be simply changed with the direction of the window.

According to our demonstration, there is a threshold of laser power to initiate a jet (5). This is confirmed by observations shown in Fig. 2 A–C. No streaming was observed at a low power of 6.3 mW, but a substantial streaming can be seen at a power of 10 mW, and becomes even stronger at 40 mW. Our previous study also indicates that the jet size is weakly dependent on laser spot size (5). That observation is still valid, but the size and shape of a jet are clearly affected by more factors. First, from Fig. 2 B and C, we can see that jet speed is an important factor: Jets with high speeds start off with a smaller initial diameter and are less divergent as they move forward. Second, a large laser spot or micropump, as indicated by a wide yellow fluorescence path in Fig. 2D, can make a jet less divergent and more collimated in the far field, but the initial jet size can still be as small as in Fig. 2C. These observations can be roughly understood from the stream lines of the jets as well as the interplay between fluid mass conservation, inertia, and acoustic radiation forces. When a fast jet is launched from the window, the water must be supplied from its surrounding region, which makes the jet originate from the center of a laser spot and have an initial size much smaller than the laser spot. Once the jet leaves the window, its motion is governed by the inertia of the fluid and acoustic radiation forces. Because a larger laser spot produces a more collimated ultrasound wave (8), the streaming becomes less divergent.

The instantaneous action of a micropump without photoacoustic cavity preparation has given us unprecedented freedom to create micropump patterns and various fluid movements (21). We can

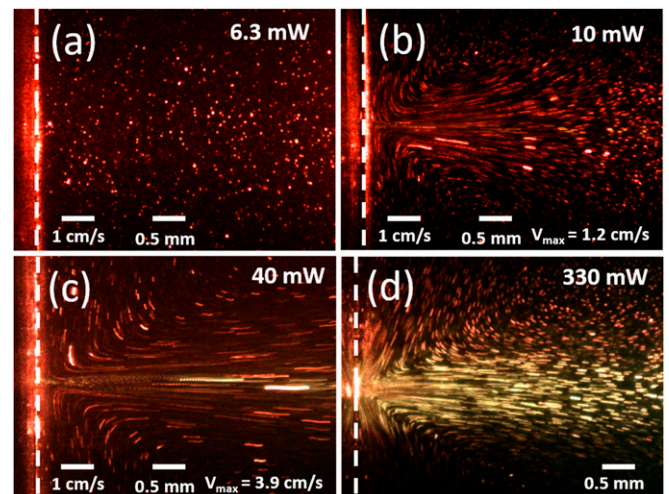


Fig. 2. Jet-stream pattern by micropumps under different laser powers and spot sizes. (A–C) Laser spot size of 50- μ m diameter and laser power of (A) 6.3 mW, (B) 10 mW, and (C) 40 mW. (D) Laser power of 330 mW and spot size of 300 μ m \times 50 μ m.

create a sweeping micropump as we sweep a laser beam (Fig. 3 *A–C*). Because of the inertia of the fluid, a moving jet cannot reach as far as a steady jet does. To generate two micropumps/jets at the same time, we simply split the beam into two. Fig. 3 *D–F* shows that two jets are generated by two beams, and the strength of each jet can be independently controlled by each beam. However, due to proximity of the two jets, they either merge into a wider jet when both are equally strong (Fig. 3 *E*), or a weaker jet is swallowed by a stronger one as in Fig. 3 *D* and *F*. If we consider each jet as one fountain, we can create all kinds of dancing fountains simply by playing with laser beams.

The on-demand jet generation and controlled generation of laser pulses further allow us to explore the mechanism of pumping by examining a single laser pulse's jet. Fig. 4 shows a sequence of high-speed images of fluid at every 20 ms before and after the striking of a laser pulse. It can be seen from Fig. 4 *A* that the fluid is almost stationary initially. The fluid begins to move only after the arrival of a laser pulse, as indicated by the green color of some tracing particles in Fig. 4 *B*. However, unlike movement near the window in a continuous streaming, the water near the window remains motionless. The region with the highest fluid speed is about ~ 1 mm away from the window, as marked by the green box in Fig. 4 *B*. Fig. 4 *E* and *F* further shows that the fluid speed quickly decreases and becomes very small after 40 ms. Such a detailed picture of the dynamics of acoustic streaming, or Eckart streaming to be precise (22), has not been reported, although some studies on transient acoustic streaming have appeared (10, 11).

In addition to steady-state stream lines and average flow speed, detailed inspection of the trajectories of tracing particles provides us more information about the local instantaneous speed of particle along its trajectory. This is because during the 10-ms exposure time for each image, the camera is constantly recoding the position of particles. The fluorescent intensity of a pixel is proportional to the time a particle spends in one position. For a motionless particle, it appears as a bright spot in the image;

for a fast-moving particle, the trace is dimmer because of low exposure time, but for a slowly moving particle, the trace appears brighter because of increased exposure time for each pixel. In principle, the integrated fluorescent intensity from a particle trajectory is the same no matter if it is moving or not because the total fluorescent- or scattered light is the same for the same exposure time. Such a correlation can be verified by trajectories in Fig. 4 *A*, *E*, and *F*. The tracer particles appear bright when they are not moving. Because of the decelerating stream in Fig. 4 *E* and *F*, the trajectories become dimmer at the left side (beginning) but brighter on the right side (end).

With this correlation in mind, let us take a closer look at the traces in Fig. 4 *B*, and especially at two trajectories indicated by yellow arrows. The trajectories begin with green spots and bright-red color, become dimmer in the first 1/5 of their paths (indicated by the tips of yellow arrows), but after that, the trajectories become stronger and stronger. These color and intensity codes give us a vivid picture of the dynamics of a jet: The fluid begins to accelerate shortly after the strike of the laser pulse and quickly reaches its maximum speed, as revealed by a weaker trajectory. After that, the speed of fluid begins to decrease, as indicated by stronger trajectories. This picture agrees well with our current understanding of photoacoustic laser streaming (5). An ultrasound pulse will be generated immediately when the laser hits the quartz window, but it will take about $0.5 \mu\text{s}$ to reach the two tracing particles. This time delay can be neglected compared with the 10-ms total exposure time. According to the principles of acoustic streaming, the volumetric force exerted on fluid is proportional to the ultrasound intensity and is in the same direction as ultrasound propagation. Because the ultrasound will last for about 0.5 ms (5), it is safe to assume that the fluid gets accelerated during this period and reaches the highest speed at the end of ultrasound. The damping of fluid begins after the passing of the ultrasound; that is why we see the green laser first, followed by a short period of acceleration, and then a longer period of deceleration.

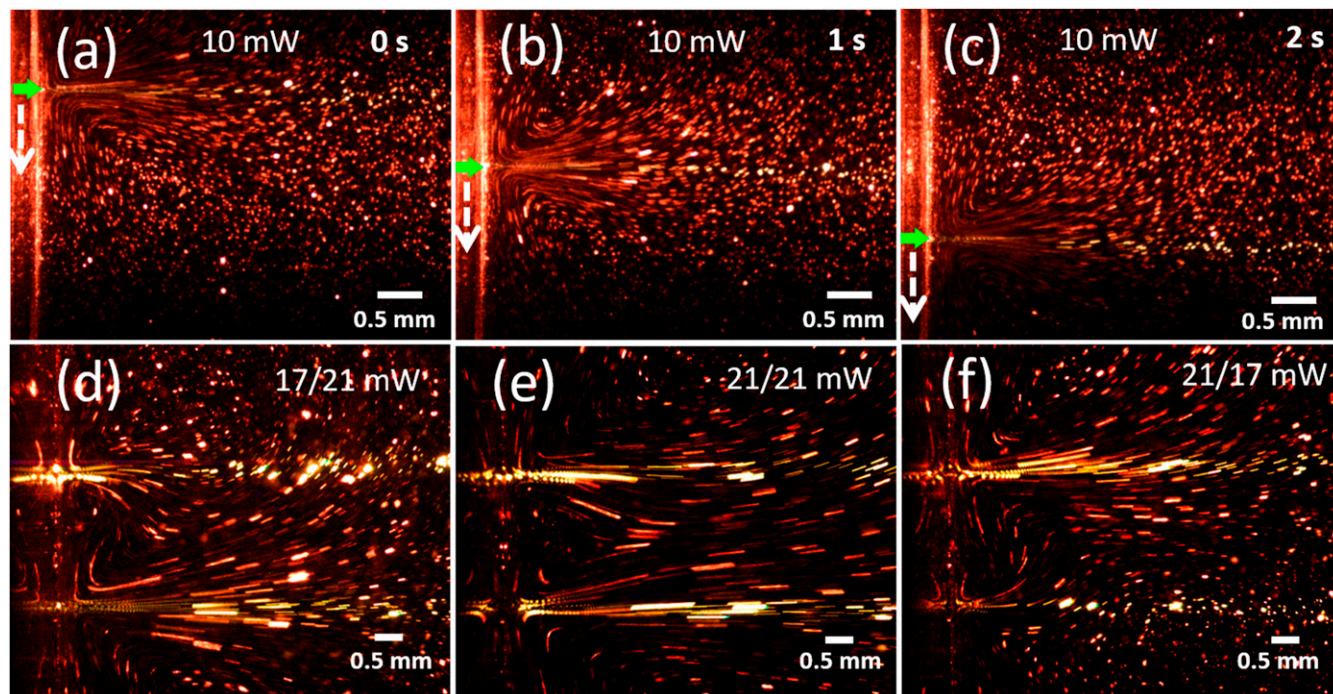


Fig. 3. A moving micropump and double micropumps. (*A–C*) Snapshots of streaming at 0, 1, and 2 s when a laser beam is moving downward at a speed of ~ 1 mm/s. Green arrows indicate the positions of laser spots, and white arrows show the laser spot's velocity direction. (*D–F*) Streaming by two laser beams with different up/down laser powers.

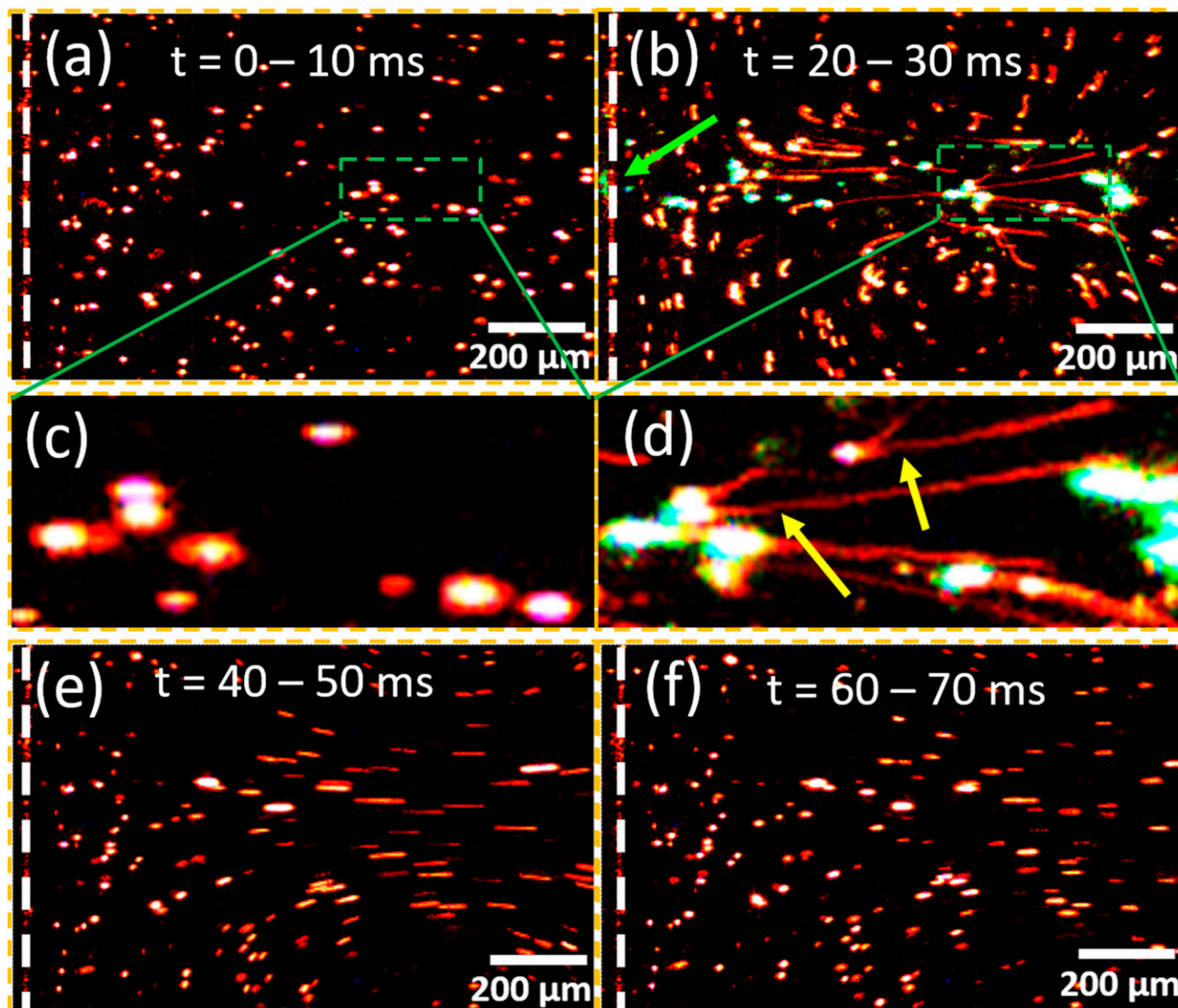


Fig. 4. Creation of a jet by a single laser pulse. The long-pass filter was removed so that green light from laser pulses can also be observed. (A, B, E, and F) Time-sequenced snapshots of fluid motion before and after a laser pulse. Exposure time is 10 ms. The green arrow in B indicates the laser's focused spot on the quartz plate. The bright-white color of microspheres is due to strong fluorescence and CCD saturation. (C and D) Zoomed-in images of the regions indicated by boxes in A and B. Laser pulse energy: 0.5 mJ.

Fig. 5 summarizes our observation and understanding of photoacoustic micropumping from the Au quartz window. The mechanism is the same photoacoustic streaming as before except that Au nanoparticles/clusters are now embedded in the quartz surface layer instead of being attached to the cuvette cavity surface. Again, the key to the success of laser streaming is that a long-lasting ultrasound wave can be generated by a single laser pulse (5). Laser-induced heating and photothermal expansion of the embedded Au particles induces a stress inside the quartz plate and causes ultrasonic vibrations of the quartz plate. Such a local surface vibration and heating will induce vibration of water in two directions: longitudinal vibration normal to the quartz surface and shear vibration parallel to the surface. However, the shear motion of the plate cannot be effectively propagated into the liquid because this motion decays exponentially in the liquid and the penetration distance is typically less than 1 μm at room temperature (23). Only the longitudinal vibrations of the quartz plate can be effectively propagated

through the liquid. This vibration induces a longitudinal ultrasonic wave in the liquid, leading to a liquid jet normal to the plate surface (24, 25).

A clear picture of the formation of a jet by a single pulse has given us strong evidence to disqualify alternative theories for laser-induced pumping or streaming. The possibility of jet by bubble cavitation, laser ablation, or laser-induced forward transfer can be immediately eliminated because no microbubble, no cavitation, and no plume is observed (26–31). Most importantly, all these theories imply that a jet should be launched from the surface of the quartz window; in other words, the fluid near the window surface should have the highest speed. This implication clearly contradicts our observation that the fluid remains motionless there despite it being in direct contact with the vibrating quartz surface. The same argument of single pulse jet formation can be applied to acoustophoresis, photophoresis, and other phenomena by which tracing microspheres should be pushed forward first and then will drag fluid along (6, 7, 32–36). Since neither the

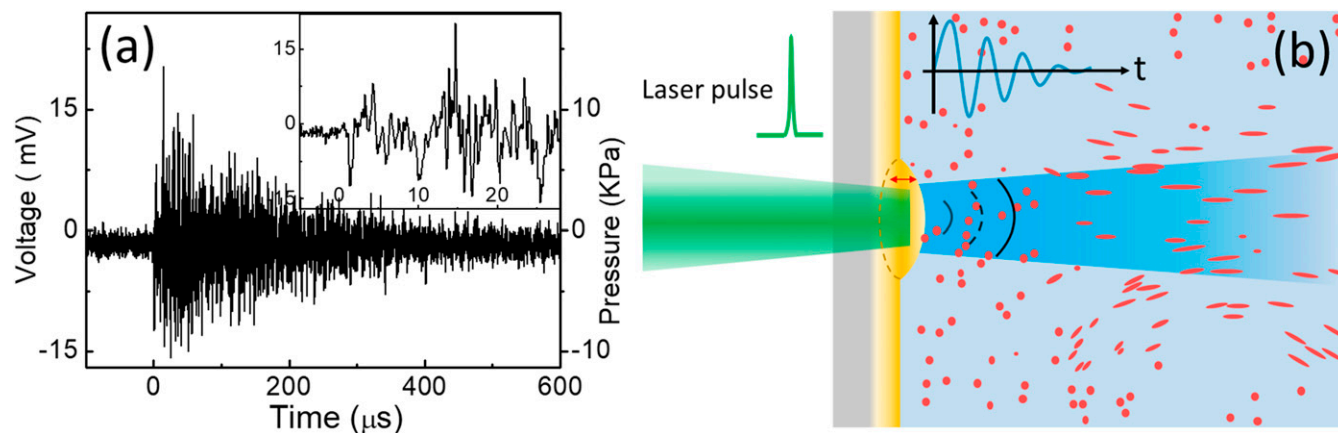


Fig. 5. Mechanism of photoacoustic micropumping. (A) Typical long-lasting photoacoustic oscillation excited by a single laser pulse. The converted pressure from hydrophone voltage signal is shown on the right axis. (Inset) The hydrophone signal for the first 30 μs . (B) Schematic of photoacoustic wave and streaming. The absorption of incident laser makes the surface layer expand thermally and vibrate mechanically, leading to an ultrasound wave. The streamlines are based on Fig. 4E, ~ 20 ms after the laser pulse.

microspheres nor the fluid near the windows exhibit any obvious movement, those theories do not hold true.

Although the principle of photoacoustic microfluidic pumps has been established, the technique was not ready for microfluidic application (5). First, plasmonic nanoparticle aqueous suspension has to be used to fabricate a photoacoustic cavity and must be removed once the cavity is finished. Second, such a fabricated cavity cannot be used with a different laser beam because of potentially poor optical alignment. Finally, only one cavity is created each time at specific position; multiple cavities will require multiple beams to avoid optical misalignment between a cavity and the laser beam that creates it. It would be convenient to simply coat a quartz plate with Au film by thermal evaporation; however, due to the weak attachment to the substrate, the Au film will be quickly removed by laser ablation or laser-induced forward transfer (5, 28–31). All of the above limitations are overcome by implanting Au into a quartz plate to create a launch pad for long-lasting photoacoustic microfluidic pumps.

Conclusions

To summarize, we fabricated a photoacoustic window by Au implantation in a quartz substrate and used it as a launch pad for micropumps to drive liquid flows. A static pump, a moving

pump, and two alternating micropumps are demonstrated as simple examples of reconfigurable and programmable control by laser. The fabrication-free micropumps allowed us to further understand the pumping mechanism and complicated interactions between laser pulses, plasmonic structures, ultrasound, and fluid dynamics. Note that the principle of photoacoustic streaming is generalizable; many light-absorbing materials are available for the generation of photoacoustic waves such as carbon-nanotubes or carbon-based composites (37, 38), Au nanoparticles (39–43), graphene (44), MoS_2 nanocomposite (45), semiconducting polymers (46), and dye molecules (47). For compact integration, semiconductor laser diodes can be used to excite photoacoustic materials (48–50). As such, our demonstration marks the beginning of a generation of micropumps, opens up their broader applications in optofluidics and microfluidics (22, 51–55).

ACKNOWLEDGMENTS. J.B. acknowledges support from Welch Foundation (Grant E-1728) and National Science Foundation (Grant EEC-1530753). F.L. acknowledges support from China Scholarship Council. Q.Z. acknowledges support from National Natural Science Foundation of China (Grant 61805071).

- Wang YN, Fu LM (2018) Micropumps and biomedical applications—A review. *Microelectron Eng* 195:121–138.
- Laser DJ, Santiago JG (2004) A review of micropumps. *J Micromech Microeng* 14: R35–R64.
- Nguyen NT, Huang XY, Chuan TK (2002) MEMS-micropumps: A review. *J Fluids Eng* 124:384–392.
- Ashraf MW, Tayyaba S, Azfulpurkar N (2011) Micro electromechanical systems (MEMS) based microfluidic devices for biomedical applications. *Int J Mol Sci* 12: 3648–3704.
- Wang Y, et al. (2017) Laser streaming: Turning a laser beam into a flow of liquid. *Sci Adv* 3:e1700555.
- Matsuda K, Kamakura T, Maezawa M (2006) Local control of Eckart streaming near focus of concave ultrasound source with two coaxially arranged transducers. *Jpn J Appl Phys* 45:4448–4452.
- Dentry MB, Yeo LY, Friend JR (2014) Frequency effects on the scale and behavior of acoustic streaming. *Phys Rev E Stat Nonlin Soft Matter Phys* 89:013203.
- Moudjed B, Botton V, Henry D, Ben Hadid H, Garandet JP (2014) Scaling and dimensional analysis of acoustic streaming jets. *Phys Fluids* 26:093602.
- Moudjed B, et al. (2015) Near-field acoustic streaming jet. *Phys Rev E Stat Nonlin Soft Matter Phys* 91:033011.
- Muller PB, Bruus H (2015) Theoretical study of time-dependent, ultrasound-induced acoustic streaming in microchannels. *Phys Rev E Stat Nonlin Soft Matter Phys* 92: 063018.
- Hoyos M, Castro A (2013) Controlling the acoustic streaming by pulsed ultrasounds. *Ultrasonics* 53:70–76.
- Epie EN, Scott D, Chu WK (2017) Manipulating the optical properties of dual implanted Au and Zn nanoparticles in sapphire. *Photon Nanostruct* 27:17–23.
- Charnvanichborikarn S, Wong-Leung J, Williams JS (2009) Self-assembled Au nanoparticles in SiO_2 by ion implantation and wet oxidation. *J Appl Phys* 106:103526.
- Stepanov AL (2010) Synthesis of silver nanoparticles in dielectric matrix by ion implantation: A review. *Rev Adv Mater Sci* 26:1–29.
- Liu JR, Wang XM, Shao L, Chen H, Chu WK (2002) Non-linear effect of gold cluster ion induced damage in silicon. *Nucl Instrum Methods Phys Res B* 197:101–106.
- Oldenburg SJ, Averitt RD, Westcott SL, Halas NJ (1998) Nanoengineering of optical resonances. *Chem Phys Lett* 288:243–247.
- Govorov AO, Richardson HH (2007) Generating heat with metal nanoparticles. *Nano Today* 2:30–38.
- Link S, Wang ZL, El-Sayed MA (1999) Alloy formation of gold-silver nanoparticles and the dependence of the plasmon absorption on their composition. *J Phys Chem B* 103: 3529–3533.
- Schroll RD, Wunnenburger R, Casner A, Zhang WW, Delville JP (2007) Liquid transport due to light scattering. *Phys Rev Lett* 98:133601.
- Zhdanov A, Rao S, Fedyanin A, Petrov D (2009) Experimental analysis of recoil effects induced by fluorescence photons. *Phys Rev E Stat Nonlin Soft Matter Phys* 80:046602.
- Cambonie T, Moudjed B, Botton V, Henry D, Ben Hadid H (2017) From flying wheel to square flow: Dynamics of a flow driven by acoustic forcing. *Phys Rev Fluids* 2:123901.
- Wiklund M, Green R, Ohlin M (2012) Acoustofluidics 14: Applications of acoustic streaming in microfluidic devices. *Lab Chip* 12:2438–2451.
- Kanazawa KK, Gordon JG (1985) Frequency of a quartz microbalance in contact with liquid. *Anal Chem* 57:1770–1771.

24. Collins DJ, Ma Z, Ai Y (2016) Highly localized acoustic streaming and size-selective submicrometer particle concentration using high frequency microscale focused acoustic fields. *Anal Chem* 88:5513–5522.
25. Wu WH, Zhai W, Hu HB, Wei BB (2017) Acoustic field and convection pattern within liquid material during ultrasonic processing. *Acta Physica Sinica* 66:194303.
26. Mason TJ (1997) Ultrasound in synthetic organic chemistry. *Chem Soc Rev* 26:443–451.
27. Obreschkow D, et al. (2011) Universal scaling law for jets of collapsing bubbles. *Phys Rev Lett* 107:204501.
28. de Matos JB, Destro MG, da Silveira CAB, Rodrigues NAS (2014) Neutral atomic jet generation by laser ablation of copper targets. *Rev Sci Instrum* 85:083505.
29. Phipps C, Luke J, Lippert T, Hauer M, Wokaun A (2004) Micropropulsion using a laser ablation jet. *J Propuls Power* 20:1000–1011.
30. Fernandez-Pradas JM, et al. (2017) Laser-induced forward transfer: Propelling liquids with light. *Appl Surf Sci* 418:559–564.
31. Banks DP, Grivas C, Mills JD, Eason RW, Zergioti I (2006) Nanodroplets deposited in microarrays by femtosecond Ti: Sapphire laser-induced forward transfer. *Appl Phys Lett* 89:193107.
32. Barnkob R, Augustsson P, Laurell T, Bruus H (2012) Acoustic radiation- and streaming-induced microparticle velocities determined by microparticle image velocimetry in an ultrasound symmetry plane. *Phys Rev E Stat Nonlin Soft Matter Phys* 86:056307.
33. Wang W, Duan WT, Ahmed S, Mallouk TE, Sen A (2013) Small power: Autonomous nano- and micromotors propelled by self-generated gradients. *Nano Today* 8: 531–554.
34. Lu J, et al. (2017) Light-induced pulling and pushing by the synergic effect of optical force and photophoretic force. *Phys Rev Lett* 118:043601.
35. Smalley DE, et al. (2018) A photophoretic-trap volumetric display. *Nature* 553: 486–490.
36. Shvedov VG, et al. (2010) Giant optical manipulation. *Phys Rev Lett* 105:118103.
37. Baac HW, et al. (2012) Carbon-nanotube optoacoustic lens for focused ultrasound generation and high-precision targeted therapy. *Sci Rep* 2:989.
38. Hsieh BY, et al. (2015) A laser ultrasound transducer using carbon nanofibers-polydimethylsiloxane composite thin film. *Appl Phys Lett* 106:021902.
39. Ju H, Roy RA, Murray TW (2013) Gold nanoparticle targeted photoacoustic cavitation for potential deep tissue imaging and therapy. *Biomed Opt Express* 4:66–76.
40. Prost A, Poisson F, Bossy E (2015) Photoacoustic generation by a gold nanosphere: From linear to nonlinear thermoelastics in the long-pulse illumination regime. *Phys Rev B Condens Matter Mater Phys* 92:115450.
41. Chow CM, et al. (2011) Broadband optical ultrasound sensor with a unique open-cavity structure. *J Biomed Opt* 16:017001.
42. Yang X, Stein EW, Ashkenazi S, Wang LV (2009) Nanoparticles for photoacoustic imaging. *Wiley Interdiscip Rev Nanomed Nanobiotechnol* 1:360–368.
43. Chen SL, et al. (2014) Efficient real-time detection of terahertz pulse radiation based on photoacoustic conversion by carbon nanotube nanocomposite. *Nat Photonics* 8: 537–542.
44. Toumia Y, et al. (2016) Graphene meets microbubbles: A superior contrast agent for photoacoustic imaging. *ACS Appl Mater Interfaces* 8:16465–16475.
45. Lee H, et al. (2016) Nanocomposites of molybdenum disulfide/methoxy polyethylene glycol-co-polypyrrole for amplified photoacoustic signal. *ACS Appl Mater Interfaces* 8: 29213–29219.
46. Lyu Y, et al. (2016) Intraparticle molecular orbital engineering of semiconducting polymer nanoparticles as amplified theranostics for in vivo photoacoustic imaging and photothermal therapy. *ACS Nano* 10:4472–4481.
47. Kim G, et al. (2007) Indocyanine-green-embedded PEBBLEs as a contrast agent for photoacoustic imaging. *J Biomed Opt* 12:044020.
48. Maslov K, Wang LV (2008) Photoacoustic imaging of biological tissue with intensity-modulated continuous-wave laser. *J Biomed Opt* 13:024006.
49. Tajima T, Okabe Y, Tanaka Y, Seyama M (2017) Linearization technique for dual-wavelength CW photoacoustic detection of glucose. *IEEE Sens J* 17:5079–5086.
50. Allen TJ, Beard PC (2013) Light emitting diodes as an excitation source for biomedical photoacoustics. *Photons Plus Ultrasound: Imaging and Sensing 2013, Proceedings of SPIE*, eds Oraevsky AA, Wang LV (SPIE-The International Society for Optical Engineering, Bellingham, WA), Vol 8581, p 85811f.
51. Baigl D (2012) Photo-actuation of liquids for light-driven microfluidics: State of the art and perspectives. *Lab Chip* 12:3637–3653.
52. Leach J, Mushfique H, di Leonardo R, Padgett M, Cooper J (2006) An optically driven pump for microfluidics. *Lab Chip* 6:735–739.
53. Hellman AN, et al. (2007) Laser-induced mixing in microfluidic channels. *Anal Chem* 79:4484–4492.
54. Schmid L, Wixforth A, Weitz DA, Franke T (2012) Novel surface acoustic wave (SAW)-driven closed PDMS flow chamber. *Microfluid Nanofluidics* 12:229–235.
55. Stone HA, Stroock AD, Ajdari A (2004) Engineering flows in small devices: Microfluidics toward a lab-on-a-chip. *Annu Rev Fluid Mech* 36:381–411.